Crack Growth Rate Measurement of As-received and Warm-rolled 316L Austenitic Stainless Steel in Primary Water Condition of Pressurized Water Reactor

K.J. Choi [a], S.C. Yoo [a], T. Kim [a], M.J. Choi [b], S.S. Hwang [b], and J.H. Kim [a]*
[a]*Ulsan National Institute of Science and Technology (UNIST), School of Mechanical and Nuclear Engineering, Republic of Korea*
[b]*Korea Atomic Energy Research Institute (KAERI), Nuclear Materials Safety Research Division, Daejeon, Republic of Korea*
[*]*Corresponding author: kimjh@uinst.ac.kr*

1. Introduction

Irradiation assisted stress corrosion cracking (IASCC) of the internals in a pressurized water reactor (PWR) has been considered critical for long-term operation. IASCC typically occurs at doses between 0.5 dpa (for boiling water reactors, BWRs) and 2–3 dpa (for pressurized water reactors, PWRs) [1-2], and it can be expected that many NPPs are exposed to the risk of IASCC.

Irradiation produces defects, and defect clusters in grains alter dislocation and dislocation loop structures and produce defect–impurity and defect–cluster–impurity complexes, leading to radiation-induced hardening [1-8].

Irradiation also leads to changes in the stability of second-phase precipitates and to the local alloy chemistry near grain boundaries, precipitates, and defect clusters. Grain boundary microchemistry that differs significantly from bulk composition can be produced in association with both radiation-induced segregation and thermally driven segregation of alloying and impurity elements.

Irradiation damages such as radiation-induced segregation, second-phase hardening, and radiation-induced hardening make steels more susceptible to IASCC.

The radiation damages were increased by long-term operation which consequently results in the increase of degradation of reactor internals such as IASCC. In fact, some cracking of the internals such as guide tube support pin and baffle former bolt in operation PWR plants has already been identified since 1985.

Of the internals, baffle-former bolts (which assemble formers and baffles) exhibit relatively high susceptibility to irradiation-assisted stress corrosion cracking due to the relatively high irradiation does and tensile stress occurring after the assembly of the formers and baffles.

And, with the extension of PWR's design life or continued operation, more careful study on the integrity of the internal structures needs to be pursued.

In addition, it has been recently reported that stress corrosion cracking (SCC) susceptibility for Ni base alloy depends on the dissolved hydrogen (DH), and the SCC susceptibility has the maximum under the environment around 10 cm^3/kg of DH where the Ni/NiO phase transition exists [9-10]. In the other words, the peak of stress corrosion rates occurring at the phase transition tends to decrease symmetrically as delta EcP values move away from the Ni/NiO phase transition [11-12].

In order to reduce the susceptibility of the alloy to SCC, there has been a tendency to increase DH of the primary section of pressurized water power plants up to approximately 50 cm^3/kg.

Although 50 cm^3/kg of DH can reduce the susceptibility to stress corrosion cracking in Ni base alloy, it may aggravate the susceptibility of stainless steel to SCC [13-15].

Warm-rolling and heat-treatment were applied to 316L stainless steel, in order to simulate the effect of radiation damage such as hardening and radiation-induced grain boundary segregation.

In summary, in this study, it is objective to investigate the effects of dissolved hydrogen concentration and warm rolling on crack growth rate of austenitic stainless steel, the crack growth rate testing and characterization of oxide structure were performed at high temperature hydrogenated water condition.

As the results, warm-rolled specimens showed higher crack growth rate than as-received one since slip band and dislocation, which were formed during warm rolling, played roles as the path for corrosion and cracking.

Also, crack growth rate increased as the dissolved hydrogen concentration increases.

It may be contributed from dropped performance and stability of protective oxide layer.

2. Experimental Procedure

To investigate the effects of dissolved hydrogen and warm rolling on crack growth rate, a plate of austenitic stainless steel 316L was used; its composition is

presented in Table 1. Figure 1 illustrates the heat treatment and the warm rolling process, which were used to simulate radiation damage, such as radiation-induced segregation and radiation-induced hardening. Once, heat treatment was performed to simulate chromium depletion in grain boundary, which seems similar with radiation induced segregation. Then, warm rolling was performed to simulate hardening. Although there are other methods (such as cold working) to simulate hardening, warm rolling was selected to not cause the unfavorable microstructural phase (e.g. martensitic phase) which is not observed in irradiated stainless steel [16-17].

For these reasons, heat treatment was performed at 630℃ for 100 h. Then, 20% of warm rolling at 250℃ was conducted in the 'c' direction (first step), followed by 20% of warm rolling in the 'a' and 'b' directions (second and third steps).

Finally, 30% of warm rolling was conducted in the 'c' direction (fourth step).

All the warm rollings were performed at 250℃. In this way, 20%-20%-50% warm rolled stainless steel plate was prepared. And, chromium depletion in grain boundary and hardening were confirmed through hardness, tensile test and TEM analysis.

In this study, as-received and 20%-20%-50% warm rolled stainless steels were used to evaluate the effects of dissolved hydrogen and warm rolling on crack growth rate.

Once, for the crack growth measurement, the procedure of which was determined following previous studies [18-23], as-received and 20%-20%-50% warm-rolled specimens were machined as 0.5T compact tension-type (0.5T CT) specimen with 12.5 mm thickness. 20%-20%-50% warm-rolled specimen has S-T orientation, i.e., crack growth direction parallel to main rolling direction ('c' direction or T direction) as shown in Fig. 3.

The as-received and 20%-20%-50% warm-rolled were machined with 5% side grooves on each side and instrumented with platinum current and potential probe leads for direct current (DC) potential drop measurements of crack length. Current flow through the sample was reversed about once per second, primarily to reduce measurement errors associated with thermocouple effects and amplifier offsets.

Zirconia sleeves and washers were used to electrically insulate the 0.5T CT specimens from the loading pins and grips. The relationship between crack length and voltage was determined according to the method of Hicks and Pickard [24].

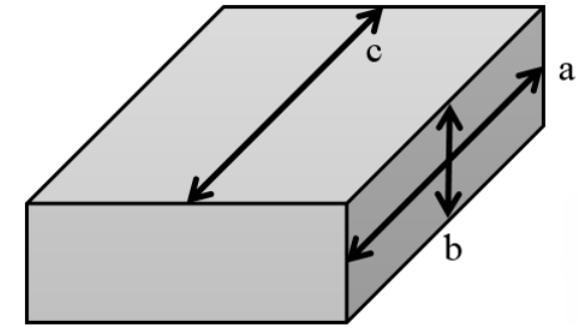

(a) Direction of Warm rolling

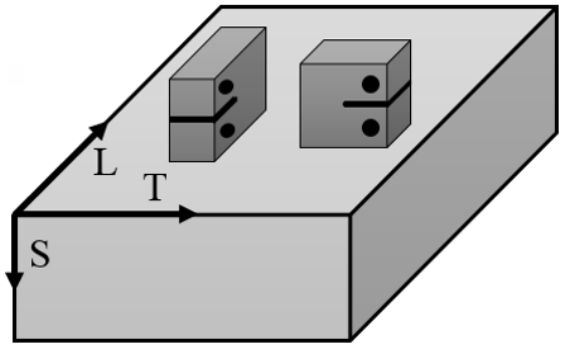

(b) Direction of Specimen

Fig. 1. Rolling direction of warm-rolled CT specimen for crack growth measurement (left: S-L & right side: S-T)

At a frequency of 1 Hz for R values of 0.3, 0.5, and 0.7, the experiment was performed at a lower Kmax than that at which the crack growth measurement was performed. Subsequently, pre-cracking for sharpening of machined notch was executed at R = 0.7 and frequencies of 0.1 and 0.01 Hz. Finally, pre-cracking was completed at a frequency of 0.001 Hz, for R = 0.7, with triangle (step 6) and trapezoidal (step 7) waveforms. These processes are described in Table 2.

Tests were conducted in an autoclave system specially constructed for the present study. Careful consideration was given for ensuring extremely rigorous chemistry control, and near-theoretical water conductivity was achieved routinely. Tests were conducted in an autoclave system specially constructed for the present study. Careful consideration was given to ensuring extremely rigorous chemistry control, and near-theoretical water conductivity was achieved routinely.

Table 1. Chemical composition and material properties of Type 316L stainless steel

Chemical composition (wt.%)												Tensile Test (MPa)	
C	Si	Mn	P	S	Cr	Ni	Cu	Al	Ti	N	Mo	Y.S.	T.S
0.016	0.49	1.38	0.033	0.002	16.6	10	0.13			0.09	2.02	276	590

Table 2. Procedures for crack growth measurement

Step	R	Waveform	Frequency (Hz)	Hold (s)	K_{max} (MPa (s
0	0.1	Sine	10		
1	0.3	Sine	1		16
2	0.5	Sine	1		18
3	0.7	Sine	1		20
4	0.7	Sine	0.1		20
5	0.7	Sine	0.01		20
6	0.7	Triangle	0.001		30
7	0.7	Trapezoidal	0.001	9,000	0
8	1	Constant	DH=25 cm³/kg		30
7	0.7	Trapezoidal	0.001	9,000	30
8	1	Constant	DH=50 cm³/kg		30

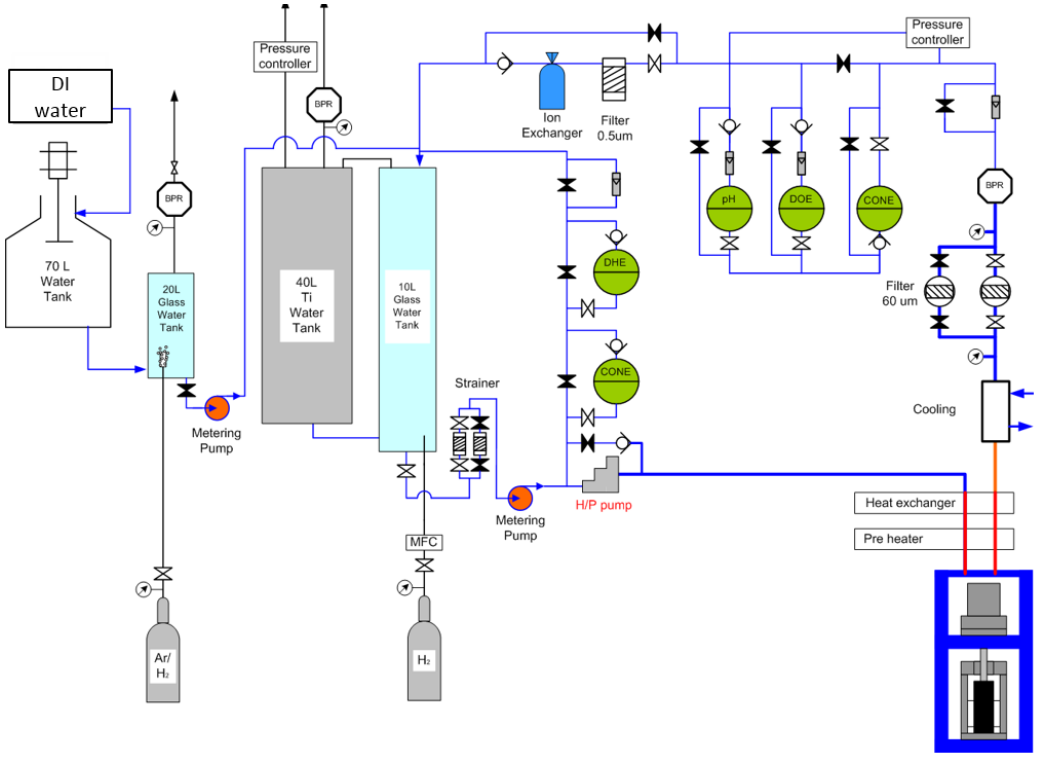

Fig. 2. Schematic of crack growth measurement

In addition to the autoclave system, a special suite of software was written to control the overall system and facilitate the measurement of crack growth and EcP using the DC potential drop technique and platinum electrode. Figure 2 presents a schematic of the autoclave system. The system is fully instrumented for oxygen, hydrogen, pH, and conductivity for both the inlet and outlet water. Distilled and demineralized water is supplied to the makeup system from the laboratory water supply system. The makeup system then circulates the water through a demineralizer/filter system to ensure cleanliness.

Makeup water is supplied through a chemistry conditioning system, where the water chemistry is adjusted, to the autoclave system. Provision has been made for injection of chemicals as well as for gas purging.

In the present study, to evaluate the effects of dissolved hydrogen and warm rolling on the susceptibility to stress corrosion crack growth, with as-received specimen, crack growth rate measurement was performed at both 25 cm³/kg and 50 cm³/kg of dissolved hydrogen. And, with 20%-20%-50% warm rolled specimen, crack growth rate measurement was performed at 25 cm³/kg dissolved hydrogen. The testes were performed in a 3.79 L stainless steel autoclave, which can maintain conditions of 1200 ppm B, 2 ppm Li, 25 and 50 cm³/kg of dissolved hydrogen, dissolved oxygen < 5 ppb, 340℃, and 17.5 MPa.

Simultaneously, after the exposure at the test environment of crack growth rate measurements for 1,000 h, the characterization of oxide film of the as-received and warm rolled specimens was performed.

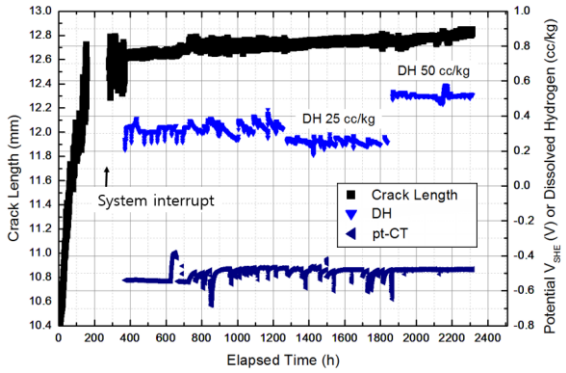

(a) Total test sequence

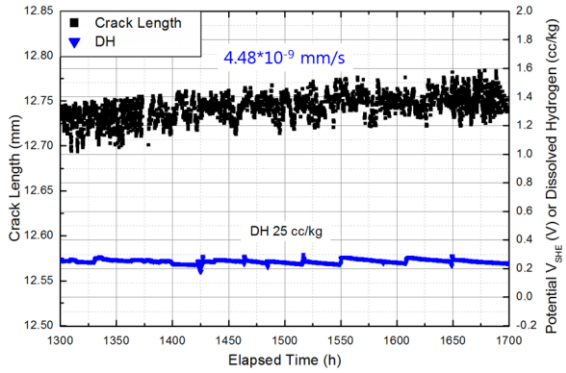

(b) Magnified view at 25 cm³/kg DH sequence

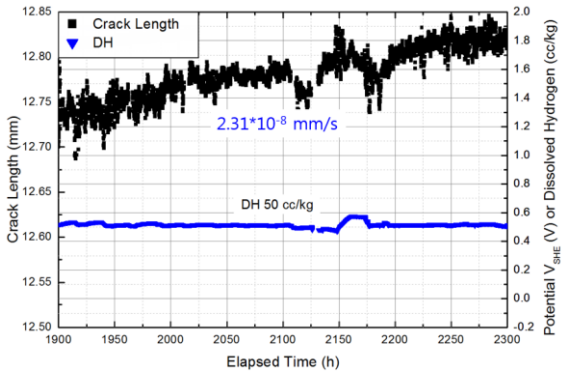

(c) Magnified view at 50 cm³/kg DH sequence

Fig. 3. Details of as-received stainless steel test results

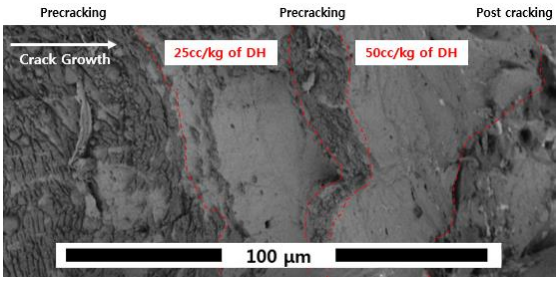

Fig. 4. Fracture surface of as-received 0.5 inch CT specimen

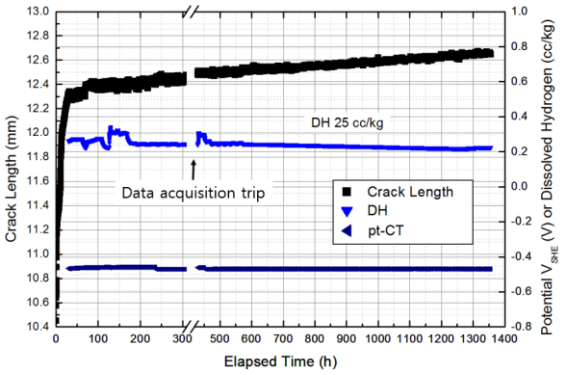

(a) Total test sequence

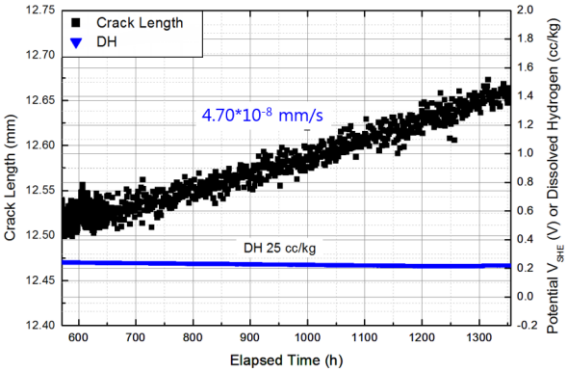

(b) Magnified view at 25 cm³/kg of DH sequence

Fig. 5. Details of warm-rolled stainless steel test results

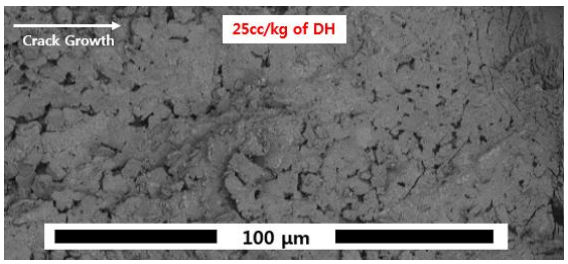

Fig. 6. Fracture surface of as-received 0.5 inch CT specimen

3. Results and Discussion

Figure 3 illustrates the results of the crack growth measurement that was performed for as-received austenitic stainless steel 316L under test conditions simulating the primary section in a PWR. The total elapsed time was 2325 h and the stabilization of water conditions was conducted after pre-cracking was performed for 420 h. At 25 cm³/kg of DH (Fig. 3(b)), the crack growth rate was found to be about $4.48E^{-9}$ mm/s, estimated in the region from 1279 h to 1750 h.

Conversely, at 50 cm³/kg of DH (Fig. 3(c)), the growth rate was found to be about $2.31E^{-8}$ mm/s, estimated in the region from 1878 h to 2325 h. At two DH conditions, the transgranular cracks were observed in Fig. 4.

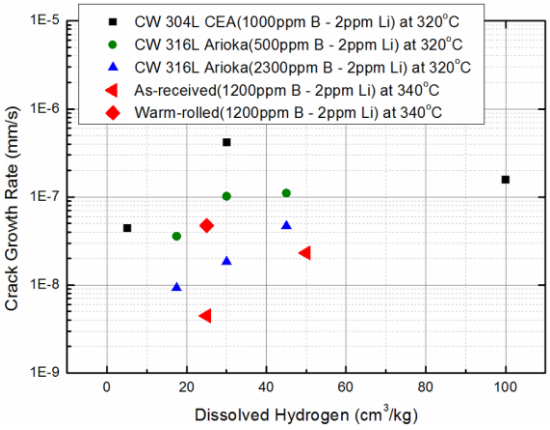

Fig. 7. Distribution of crack growth rate with DH

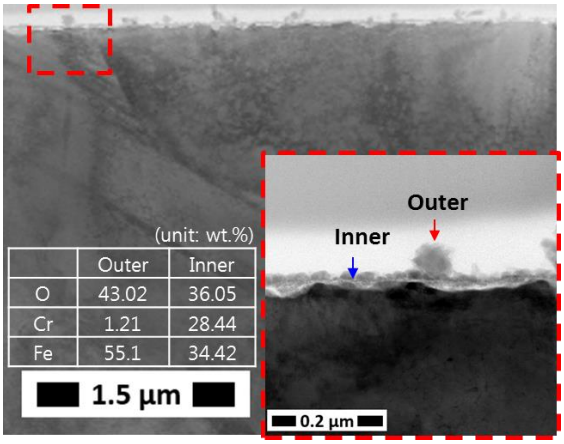

	Outer	Inner
O	43.02	36.05
Cr	1.21	28.44
Fe	55.1	34.42

(a) As-received SS exposed at 25cm³/kg of DH for 1,000 h

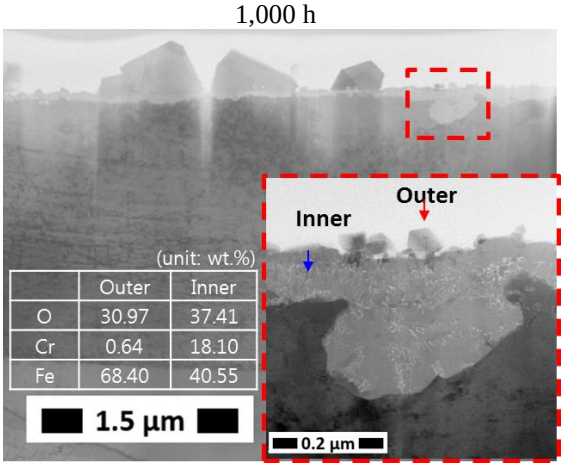

	Outer	Inner
O	30.97	37.41
Cr	0.64	18.10
Fe	68.40	40.55

(b) As-received stainless steel exposed at 50cm³/kg of DH for 1,000 h

Fig. 8. Oxide structure of as-received (a) warm rolled (b) stainless steel exposed at 25cm³/kg of DH for 1,000 h

In Fig. 5, there are the results of the crack growth measurement that was performed for 20%-20%-50% warm rolled austenitic stainless steel 316L under test conditions simulating the primary section in a PWR. The total elapsed time was 1370 h and the stabilization of water conditions was conducted after pre-cracking was performed for 570 h. At DH 25 cm³/kg (Fig. 5(b)), the crack growth rate was found to be about 2.21E-8 mm/s, estimated in the region from 570 h to 1370 h. And the crack growth rate at 50 cm³/kg of DH is 2.31E-8 mm/s. At 25 cm³/kg of DH, the transgranular crack also was observed in Fig. 6. Commonly, the measured ECP is about -470 mV at 25 cm³/kg of DH and about -482 mV at 50 cm³/kg of DH. The change of ECP with increasing DH was slight.

3.1 Effect of DH on Crack Growth

Figure 7 illustrates the distribution of crack growth rate with dissolved hydrogen for both the present study and a previous study [25], demonstrating the effect of dissolved hydrogen on stress corrosion crack growth. Based on this figure, it is clear that increase of dissolved hydrogen accelerates the crack growth rate.

In order to evaluate the effect of dissolved hydrogen concentration on corrosion resistance and SCC growth, the characterization of oxide films on the surface of as-received stainless steel, which were formed at 25 cm³/kg and 50 cm³/kg of dissolved hydrogen, was additionally performed with as-received stainless steel (as shown in Fig. 8). At both dissolved hydrogen conditions, the oxide films consist of outer layer (Fe_3O_4) and inner layer ($FeCr_2O_4$), which were confirmed through TEM-EDS analysis. Because the inner layer or Cr rich oxide has relatively non-porous structure compared to the outer layer and is thermodynamically stable, it is acknowledged that it plays an important role as a barrier to corrosion and SCC. The structure and composition of oxide film is not affected by the change of dissolved hydrogen concentration in the solution, nevertheless the thickness and the corrosion rate of the inner layer appear to increase with dissolved hydrogen. Additionally, the local dissolution was observed on surface of stainless steel exposed at 50 cm³/kg of dissolved hydrogen.

Based on the results of this study and the previous study [26], which evaluated the effect of dissolved hydrogen concentration on the corrosion resistance of stainless steel, the increases of the inner oxide layer and crack growth rate can be explained.

Firstly, with the increase of dissolved hydrogen, cathodic process can be promoted and result in a higher critical and passive current. Therefore, the protective performance of the inner oxide film can drop dramatically. In the other words, it represents that the increased dissolved hydrogen can reduce the stability of the inner oxide film. Next, ion diffusion is much easier and the iron release rate may increase as a consequence. Also, the adsorbed hydrogen atoms accelerates self-diffusion and diffusivity of cavities, and decreases the local growth rate and the stability of the passive film,

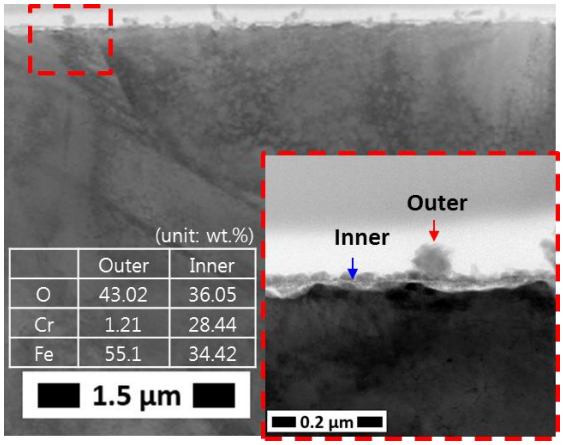

(a) As-received stainless steel exposed at 25cc/kg of DH for 1,000 h

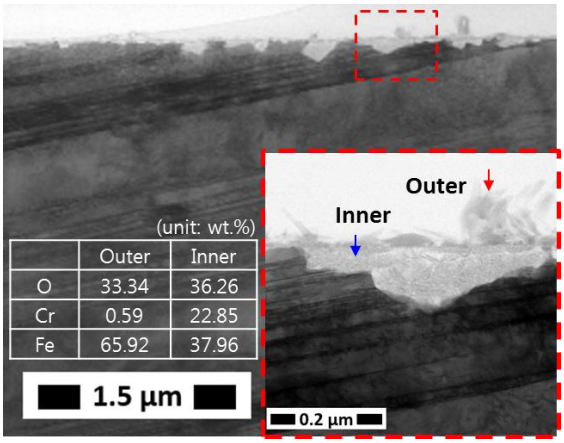

(b) Warm rolled stainless steel exposed at 50cc/kg of DH for 1,000 h

Fig. 9. Oxide structure of as-received stainless steel exposed at 25cc/kg (a) and 50cc/kg (b) of DH for 1,000 h

which can reduce markedly the effective solubility of hydrogen in a metal [27-28]. And, the corrosion may be accelerated subsequently.

Next, with the increase of dissolved hydrogen at high temperature, more H2 diffuses through the porous outer layer and comes into the inner protective layer. Then, hydrogen can be adsorbed as an atom (dissociative chemisorption) because physisorption is possible only at low temperature (less than around 25°C). The hydrogen adsorption can locally decrease the growth rate or formation rate of the inner protective layer, resulting in the formation of the un-uniform stress field [29-33]. Locally, it seems that it can cause the interruption or the formation of small crack in the inner protective layer. Actually, at 50 cm^3/kg of dissolved hydrogen (Fig. 8(b)), the empty spaces were observed in the inner protective layer. It is thought that the empty spaces were contributed to the increase of corrosion rate and oxide thickness.

In these ways, the increase of dissolved hydrogen concentration can accelerate corrosion rate of stainless steel by aggravating the stability of inner protective layer, resulting in the increase of crack growth rate.

3.2 Effect of Warm Rolling on Crack Growth

In Fig. 7, at 25 cm^3/kg of dissolved hydrogen, there are the results of crack growth rate measurements for as-received and warm rolled specimens, demonstrating the effect of warm rolling on SCC growth. Based on this figure, it is clear that the crack growth rates were increased with heat treatment and warm rolling for the simulation of radiation damages (such as radiation induced segregation and radiation hardening). Initially, because depletion of Cr in grain boundary reduces the resistance on corrosion and also induces the increased susceptible on SCC, it was expected that crack growth rate was accelerated with warm rolling [1, 15, 34]. In 20%-20%-50% warm rolled stainless steel, the increase of crack growth rate was observed through the crack growth rate measurements shown in Fig. 9.

In order to evaluate the effect of warm rolling on corrosion resistance and SCC growth, the characterization of oxide films on the surfaces of as-received and 20%-20%-50% warm rolled stainless steel, which were formed at 25 cm^3/kg of dissolved hydrogen, was additionally performed (as shown in Fig. 9). In the as-received and 20%-20%-50% warm rolled stainless steels, the oxide films consist of outer layer (Fe_3O_4) and inner layer ($FeCr_2O_4$), which were confirmed through TEM-EDS analysis. The structure and composition of oxide film is not affected by warm rolling. However, the local dissolution was observed on surface of 20%-20%-50% warm rolled stainless steel exposed at 25 cm^3/kg of dissolved hydrogen.

Instead, slip bands induced by warm rolling may attribute not only to the increase of local dissolution owing to the presence of lower bonding energy points compared to “perfect” crystals but also the linear degradation of passive film stability [35-38].

Also, Multiplication of dislocations induces high stress concentration and modifies local potential. Therefore, corrosion resistance is decreased by increased number of dislocations due to potential difference between matrix and dislocation inclusion [39-40].

Therefore, 20%-20%-50% warm rolled stainless steel, having slip bands and dislocation which play roles as the path for corrosion and crack, shows the localized corrosion on the surface (shown in Fig. 9(b). In that, warm rolled SS has the lower corrosion resistance, causing the increase of crack growth rate.

Additionally, the fracture mode was transgranular, not intergranular. It can be explained with the direction of 0.5 T specimen and warm rolling. 50% warm rolling,

on the upper side or in direction "L", resulted in the formation of slip band or dislocation, which is parallel to upper side or direction "L". It is also parallel to crack surface of CT specimen.

In the case, although 20%-20%-50% warm rolled SS has sensitized grain boundary and slip band, which are considered to play roles as the potential crack path [1], the crack is easier to grow into the path, which has more similar direction with crack. So, the slip bands, which has the direction parallel to the crack growth direction of 0.5 T specimen acted the path for cracking. The transgranular cracking was observed.

4. Conclusions

To investigate the effects of dissolved hydrogen and warm rolling on the resistance to stress corrosion crack growth of austenitic stainless steels, the crack growth measurement was performed at 25 cm^3/kg and 50 cm^3/kg of dissolved hydrogen in the simulated PWR primary water condition.

The dissolved hydrogen decreases the stability of protective oxide layer and accelerates the corrosion rate, and the growth rate at 50 cm^3/kg dissolved hydrogen was higher than that at 25 cm^3/kg dissolved hydrogen.

And, for the simulation of the radiation damages such as radiation-induced segregation and hardening, warm-rolling process was established, and the sample with warm-rolling process was tested under PWR primary water condition with 25 cm^3/kg of dissolved hydrogen. The crack growth rate was higher than one of as-received stainless steel. It may be because warm rolling causes the formations of slip band and chromium depletion, which play roles as the path for corrosion and SCC.

ACKNOWLEDGMENT

This work was financially supported by the Nuclear Power Core Technology Development Program (No. 2014151040004A & No. 20131520000140) of the Korea Institute of Energy Technology Evaluation and Planning (KETEP) funded by the Ministry of Trade Industry and Energy (MOTIE).

REFERENCES

[1] K.E. Sickafus, E.A. Kotomin and B.P. Uberuaga, Proceedings of the NATO Advanced Study Institute on Radiation Effects in Solids, Journal of Physical Chemistry, Vol.235, 2007

[2] P. Scott, Review of Irradiation Assisted Stress Corrosion Cracking, Journal of Nuclear Materials, Vol.211, p.101, 1994

[3] H.M. Chung and W.J. Shack, Irradiation Assisted Stress Corrosion Cracking Behavior of Austenitic Stainless Steels Applicable to LWR Core Internals, NUREG/CR-6892, ANL 04/10, 2006

[4] A. Jenssen, L.G. Ljungberg, J. Walmsely and S. Fisher, Importance of Molybdenum on Irradiation-assisted Stress Corrosion Cracking in Austenitic Stainless Steels, Corrosion, Vol.54, p.48, 1998

[5] E.A. Kenik, Radiation-induced Segregation in Irradiated Type 304 Stainless Steels Journal of Nuclear Materials, Vol.187, p. 239, 1992

[6] S. Nakahigashi, M. Kodama, K. Fukuya, S. Nishimura, S. Yamamoto, K. Saito and T. Saito, Effects of Neutron Irradiation on Corrosion and Segregation Behavior in Austenitic Stainless Steels Journal of Nuclear Materials, Vol.179-181, p. 1061, 1991.

[7] G.S. Was, J.T. Busby, J. Gan, E.A. Kenik. A. Jenssen, S.M. Bruemmer, P.M. Scott and P.L. Andresen, Emulation of Neutron Irradiation Effects with Protons: Validation of Principle, Journal of Nuclear Materials, Vol.300, p. 198, 2002.

[8] G.R. Odette and G. Lucas, The Effects of Intermediate Temperature Irradiation on the Mechanical Behavior of 300-series Austenitic Stainless Steels, Journal of Nuclear Materials, Vol.179-181, p. 572, 1991.

[9] T. Terachi, N. Totsuka, T. Yamada, T. Nakagawa, H. Deguchi, M. Horiuchi, and M. Oschitani, Influence of Dissolved Hydrogen on Structure of Oxide Film on Alloy 600 Formed Primary Water of Pressurized Water Reactors, Journal of Nuclear Science and Technology, Vol.40, p. 509, 2003

[10] D.S. Morton, S.A. Attanasio, J.S. Fish, M.K. Schurman, Influence of Dissolved Hydrogen on Nickel Alloy SCC in High Temperature Water, Corrosion, Vol.99, p. 447, 1999

[11] D.S. Morton, S.A. Attanasio and G.A. Young, Primary Water SCC Understanding and Characterization Through Fundamental Testing in the Vicinitiy of the Nickel/Nickel Oxide Phase Transition, LM-01K038. 2001

[12] R.A. Etien, E. Richey, D.S. Morton, and J. Eager, SCC Initiation Testing of Alloy 600 in High Temperature Water 15th International Conference on Environmental Degradation, TMS, 2011

[13] G. Furutani, N. Nakajima, T. Konishi and M. Kodama, Stress Corrosion Cracking on Irradiated 316 Stainless Steel, Journal of Nuclear Materials, Vol.288, 2001

[14] K. Arioka, Effects of Temperature, Hydrogen and Boric Acid Concentration on IGSCC Susceptibility of Annealed 316Sstainless Steel, colloque international fontevraud 5, fontevraud, france, SFEN publications, 2002

[15] D. Feron, E. Herms, B. Tanguy, Behavior of Stainless Steels in Pressurized Water Reactor Primary Circuits, Journal of Nuclear Materials, Vol.427, p.364, 2012

[16] A.H. Ramirez, C.H. Ramirez, and I. Costa, Cold Rolling Effect on the Microstructure and Pitting Resistance of the NBR ISO 5832-1 Austenitic Stainless Steel, International Journal of Electrochemical Science, Vol.8, 2013

[17] S. Roychowdhury, V. Kain, M. Gupta, and R.C. Prasad, IGSCC crack growth in simulated BWR environment – Effect of nitrogen content in non-sensitized and warm rolled austenitic stainless steel, Corrosion, Vol. 53, 2011

[18] J.H. Kim, R.G. Ballinger and P.W. Stahle, SCC Crack Growth in 316L Weld Metals in BWR Environments, Nace - International Corrosion Conference Series, March 16-20, 2008

[19] J.H. Kim and R.G. Ballinger, Stress Corrosion Cracking Crack Growth Behavior of Type 316L Stainless Steel Weld

Metals in Boiling Water Reactor Environments, Corrosion, Vol.64, 2008
[20] J.R. Hixon, J.H. Kim and R.G. Ballinger, Effect of thermal aging on SCC and mechanical properties of stainless steel weld metals, 13th International Conference on Environmental Degradation of Materials in Nuclear Power Systems 2007, Vol.3, 2007
[21] P.L. Andresen, J. Hickling, A. Ahluwalia and J. Wilson, Effects of Hydrogen on Stress Corrosion Crack Growth of Ni Alloys in High-Temperature Water, Corrosion, Vol.64, 2008
[22] P.L. Andresen, Environmental Assisted Growth Rate Response of Nonsensitized AISI 316 grade Stainless Steel in High Temperature Water, Corrosion, Vol.44, 1988
[23] K. Arioka, T. Yamada, T. Terachi and T. Miyamoto, Dependence of Stress Corrosion Cracking for Cold-Worked Stainless Steel on Temperature and Potential, and Role of Diffusion Vacancies at Crack Tips, Corrosion Science, Vol.46, p.691, 2008
[24] ASTM E647-12, "Standard Test Method for Measurement of Fatigue Crack Growth Rates" Annual Book of ASTM Standard, West Conshohocken, PA: ASTM, 2012
[25] Q. Raquer, E. Herms, F. Vaillant and T. Couvant, SCC of Cold-Worked Austenitic Stainless Steels in PWR Conditions, Advanced Materials Science, Vol.7, 2007
[26] T. Terachi, T. Yamada, T. Miyamoto, K. Arioka and K. Fukuya, Corrosion B Behavior of Stainless Steels in Simulated PWR Primary Water—Effect of Chromium Content in Alloys and Dissolved Hydrogen, J. Journal of Nuclear Science and Technology, Vol.45, p.975, 2008
[27] K. Dozaki, D. Akutagawa, N. Nagata, H. Takiguchi and K. Norring, Effects of Dissolved Hydrogen Content in PWR Primary Water on PWSCC Initiation Property, E-Journal of Advanced Maintenance, Vol.2, 2010
[28] D.S. Morton, E.O. Connor, R.A. Etien, N. Lewis and E. Richey, SCC Initiation Testing of Nickel-Based Alloys in High Temperature Water, ICG-EAC 2012
[29] T. Terachi, T. Yamada, T. Miyamoto and K. Arioka, SCC Growth Behaviors of Austenitic Stainless Steels in Simulated PWR Primary Water, Journal of Nuclear Materials, Vol.426, p.59, 2012
[30] S. Chen, M. Gao and R.P. Wei, Hydride Formation and Decomposition in Electrolytically Charged Metastable Austenitic Stainless Steels, Metallurgical and Materials Transactions A, Vol.27A, 1996
[31] J.G. Yu, J.L. Luo, C.S. Zhang and P.R. Norton, Photoelectrochemical Study of Hydrogen-Loaded Passive Film, Journal of The Electrochemical Society, Vol.150, 2003
[32] T. Terachi, K. Fuji and K. Arioka, Microstructural Characterization of SCC Crack Tip and Oxide Film For SUS 316 Stainless Steel in Simulated PWR Primary Water at 320ºC, Journal of Nuclear Science and Technology, Vol.42, 2005
[33] D.D. Macdonald, The Point Defect Model for the Passive State, Journal of The Electrochemical Society, Vol.139, 1992
[34] T.G. Gooch et al., "Weld decay in AISI 304 stainless steel", Metal Construction and British Welding Journal, Vol.3, 1971
[39] K. Arioka, T. Yamada, T. Terachi and G. Chiba., Influence of Carbide Precipitation and Rolling Direction on Intergranular Stress Corrosion Cracking of Austenitic Stainless Steels in Hydrogenated high-Temperature Water, Corrosion, Vol.62, 2006
[40] L. Peguet, B. Malki and B. Baroux, Influence of Cold Working on the Pitting Corrosion Resistance of Stainless Steels, Corrosion Science, Vol.49, p.1933, 2007